JOURNAL OF GEOPHYSICAL RESEARCH, VOL. 114, E11012, doi:10.1029/2009JE003428, 2009



# Aeolian dunes as ground truth for atmospheric modeling on Mars

Rosalyn K. Hayward,[1] Timothy N. Titus,[1] Timothy I. Michaels,[2] Lori K. Fenton,[3] Anthony Colaprete,[4] and Philip R. Christensen[5]

Received 8 May 2009; revised 19 July 2009; accepted 17 August 2009; published 25 November 2009.

[1] Martian aeolian dunes preserve a record of atmosphere/surface interaction on a variety of scales, serving as ground truth for both Global Climate Models (GCMs) and mesoscale climate models, such as the Mars Regional Atmospheric Modeling System (MRAMS). We hypothesize that the location of dune fields, expressed globally by geographic distribution and locally by dune centroid azimuth (DCA), may record the long-term integration of atmospheric activity across a broad area, preserving GCM-scale atmospheric trends. In contrast, individual dune morphology, as expressed in slipface orientation (SF), may be more sensitive to localized variations in circulation, preserving topographically controlled mesoscale trends. We test this hypothesis by comparing the geographic distribution, DCA, and SF of dunes with output from the Ames Mars GCM and, at a local study site, with output from MRAMS. When compared to the GCM: 1) dunes generally lie adjacent to areas with strongest winds, 2) DCA agrees fairly well with GCM modeled wind directions in smooth-floored craters, and 3) SF does not agree well with GCM modeled wind directions. When compared to MRAMS modeled winds at our study site: 1) DCA generally coincides with the part of the crater where modeled mean winds are weak, and 2) SFs are consistent with some weak, topographically influenced modeled winds. We conclude that: 1) geographic distribution may be valuable as ground truth for GCMs, 2) DCA may be useful as ground truth for both GCM and mesoscale models, and 3) SF may be useful as ground truth for mesoscale models.

**Citation:** Hayward, R. K., T. N. Titus, T. I. Michaels, L. K. Fenton, A. Colaprete, and P. R. Christensen (2009), Aeolian dunes as ground truth for atmospheric modeling on Mars, *J. Geophys. Res.*, *114*, E11012, doi:10.1029/2009JE003428.

## 1. Introduction

[2] Sand dunes are among the most widespread aeolian features present on Mars. They preserve a unique record of the interaction between the atmosphere and surface, and therefore are valuable as ground truth for atmospheric models. Aeolian dunes form where a source of sand exists, winds of sufficient strength are available to transport the sand, and the winds subsequently weaken and deposit the sand [e.g., *Fryberger and Ahlbrandt*, 1979; *Kocurek and Havholm*, 1993; *Kocurek and Lancaster*, 1999]. Both the presence and morphology of sand dunes are sensitive to subtle shifts in wind circulation patterns and strengths. Dunes are particularly suited to comprehensive planetary studies because they are abundant over a wide range of elevations and terrain types and are well preserved. Even dunes that no longer respond to contemporary winds yield information about the conditions under which they formed. Thus dunes provide a global record of atmosphere/surface interaction. We hypothesize that the location of dune fields may record a relatively long-term integration of atmospheric activity across a relatively broad area, preserving Global Climate Model (GCM)–scale atmospheric trends. We examine location in two ways, beginning with the global geographic distribution of the dune fields. Next we calculate dune centroid azimuth (DCA; see Figure 1), a measure of the relative position of each intracrater dune field within its surrounding crater. In contrast, individual dune morphology, as expressed in slipface orientation (SF; see Figure 1), may be more responsive to localized variations in circulation, preserving topographically controlled mesoscale trends. We test this hypothesis by comparing three dune characteristics: 1) geographic distribution, 2) DCA, and 3) SF, to the NASA Ames Research Center Mars GCM (referred to hereafter as Ames Mars GCM) and to the Mars Regional Atmospheric Modeling System (MRAMS).

## 2. Background

[3] Over three decades ago, Mariner 9 and Viking images revealed Martian dune fields, allowing researchers to examine and map aeolian morphologies [*McCauley et al.*,

[1]U.S. Geological Survey, Flagstaff, Arizona, USA.
[2]Southwest Research Institute, Boulder, Colorado, USA.
[3]Carl Sagan Center, Moffett Field, California, USA.
[4]NASA Ames Research Center, Moffett Field, California, USA.
[5]Department of Geological Sciences, Arizona State University, Tempe, Arizona, USA.


0148-0227/09/2009JE003428$09.00

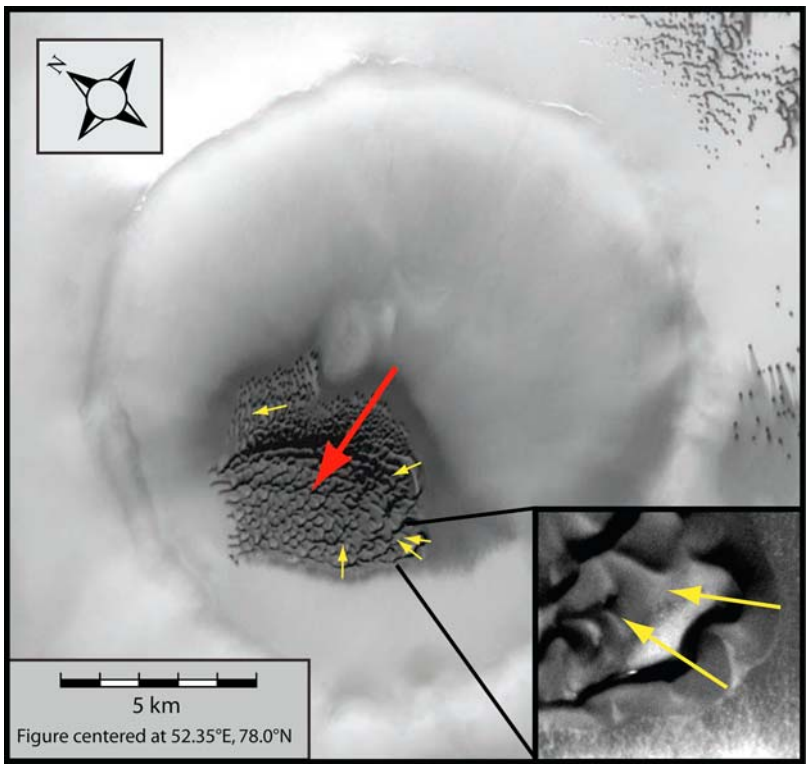


**Figure 1.** Example of DCA (red) and SF (yellow). The inset, an enlargement of the south corner of the dune field, is example of SF. Note variety of orientations of SFs within dune field. CTX image T01_000857_2581, illumination from bottom. Polar Stereographic projection.

1972; *Cutts and Smith*, 1973; *Ward et al.*, 1985] and to anticipate wind patterns [*Ward*, 1979; *Thomas*, 1982; *Greeley et al.*, 1993; *Anderson et al.*, 1999]. More recent studies, using high-resolution Mars Global Surveyor (MGS) Mars Orbiter Camera narrow angle (MOC NA) images [*Malin et al.*, 1992], Mars 2001 Odyssey Orbiter Thermal Emission Imaging System (THEMIS) visible range (VIS) images [*Christensen et al.*, 2004], and Mars Reconnaissance Orbiter (MRO) High Resolution Imaging Science Experiment (HiRISE) images [*McEwen et al.*, 2007], have enabled scientists to reexamine previously mapped dune fields and to discover new aeolian deposits unresolved by previous instruments [e.g., *Malin et al.*, 1998; *Edgett and Malin*, 2000; *Fenton et al.*, 2002, 2003; *Bourke et al.*, 2004; *Hayward et al.*, 2007a]. Higher resolution images have also allowed researchers to discern subtle details, such as slipface orientation, that improve prediction of wind patterns, [e.g., *Fenton et al.*, 2003, 2005; *Michaels*, 2008]. Previously, we compared the location and morphology of dunes between 65° S and 65° N to the Ames Mars GCM. While we observed that agreement was good between GCM and DCA, GCM and SF-derived wind direction were in poor agreement for intracrater dune fields, possibly because the SFs were being influenced by local, topographically controlled winds [*Hayward et al.*, 2007a, 2008]. *Greeley et al.* [2006, 2008] examined the orientation of aeolian features using orbiter images and concurrent surface images from cameras onboard Spirit, one of the Mars Exploration Rovers (MER). Feature orientations, when compared to both GCM and mesoscale modeled wind directions, were found to be most consistent with MRAMS modeled winds from the NW. *Sullivan et al.* [2008] found that the strongest winds during Spirit's mission, those winds that raised sand on the rover deck or caused ripple crests to migrate downwind, were the rare, stronger, SSE winds that were not as predictable or repetitive as MRAMS modeled winds. While such surface observations provide more information, the relationship between modeled wind direction and wind direction indicated by aeolian features remains unclear. Thus further examination of aeolian features and their relationship to modeled winds is important. In this study we use a Geographic Information System (GIS) to compare two scales of modeled winds to three characteristics of globally mapped dune fields. The comparison tests whether wind directions indicated by the location and morphology of dunes are consistent with wind directions simulated by the GCM and mesoscale atmospheric models of the current Mars climate.

## 3. Methods

[4] This section discusses the five elements that are being compared in our study. We begin with the modeled winds, progressing from the global scale (Ames Mars GCM) to the mesoscale (MRAMS). Next we describe the three dune characteristics, progressing from a global scale (geographic distribution), to a local scale (DCA and SF). Finally, we discuss the selection of an appropriate mescoscale model study site and describe its physical setting.

### 3.1. Modeled Winds

#### 3.1.1. GCM Wind Direction

[5] The Ames Mars GCM results used here were computed on a global, cylindrically projected grid with a grid point spacing of 5° × 6° (latitude x longitude). Output was recorded for each Martian day in one Martian year for current orbital/axial conditions. Shear stress, wind velocity and wind azimuth were provided 8 times daily [*Haberle et al.*, 1999]. We use winds with a shear stress >0.0225 N/m$^2$ for comparison to our directional data. *Haberle et al.* [2003] have demonstrated that setting a threshold stress of 0.0225 N/m$^2$ with the Ames Mars GCM will lift dust (through bombardment from sand saltation) in spatial patterns that qualitatively agree with observed dust storm occurrences. While we have chosen this threshold stress value, it is possible that sustained movement of sand may require long-term winds significantly above this threshold. If no modeled winds above the threshold exist for an area, we consider winds with a velocity > 10m/sec as indicative of potential sand transport. The height of the modeled wind velocity varies with pressure and is typically between 3 and 8 m [*Haberle et al.*, 1999]. Unless otherwise specified, when we compare GCM to DCA or SF, we consider winds within 360 km of the DCA or SF location.

#### 3.1.2. Mesoscale Model Wind Direction

[6] In contrast to the Ames Mars GCM, MRAMS [*Rafkin et al.*, 2001] uses significantly higher spatial resolution topography over a small area, so local topographic effects can be simulated (horizontal grid spacing ~550 m). Temporal resolution is also quite high. Output was recorded every 20 Martian minutes for two Martian sols (72 times per sol). Due to the high spatial and temporal resolution, it is only practical to run the simulation for 2 sols. We do not use the shear stress >0.0225N/m$^2$ threshold for mesoscale output because only ~1350 of the ~1.5 million modeled winds have a surface stress >0.0225N/m$^2$. We use the less stringent threshold of wind velocity >10 m/sec and when focusing on the dune field area, where few winds exceed 10 m/sec, we consider all winds regardless of magnitude. The height of the modeled wind velocity is 15 m above ground level.

### 3.2. Dune Characteristics

#### 3.2.1. Geographic Distribution

[7] Geographic distribution examines the location of the dune fields on a global scale and is available as a natural outgrowth of mapping the dune fields. We extract our dune location data for 65°S to 65°N from the Mars Global Digital Dune Database (MGD$^3$): MC2-MC29, available as U.S. Geological Survey (USGS) Open File Report (OFR) 2007–1158 [*Hayward et al.*, 2007b] (http://pubs.usgs.gov/of/2007/1158/). North polar (65°N to 90°N) data is taken from MGD$^3$: MC-1 (will be released as a USGS OFR in 2009). South polar (65°S to 90°S) dune data is from our preliminary work on the MC-30 portion (65°S to 90°S) of the database that will be released in 2010. MGD$^3$ was built from 100 m/pixel THEMIS infrared (IR) band 9 images covering orbits 816–9601 (02/2002–02/2004; $L_s$ = 0.085°–358.531°), comprising more than 30,000 images, providing ~75% reliable coverage planet-wide. Coverage improved for the polar areas where higher resolution (35 to 72 m/pixel) THEMIS VIS mosaics were available during mapping. Because the initial locations of dune fields are based on THEMIS IR images, only moderate to large size dune fields are included in the database, with the smallest dune field being ~ 1 km$^2$ in area. The absence of mapped dune fields does not mean that such dune fields do not exist and does not imply a lack of saltating sand in other areas. Bright, ripple-like bed forms, commonly known as transverse aeolian ridges, or TARs, [e.g., *Wilson and Zimbelman*, 2004] are not included in the database.

#### 3.2.2. Dune Centroid Azimuth

[8] Moving from a global scale to a more local scale, we look at another measure of the location of a dune field, its relative position within a crater. DCA is the geodesic azimuth of the line connecting the centroid (geographic center) of the crater to the centroid of the dune field (Figure 1). Relative position within the crater might indicate the prevailing wind direction during the period of dune field migration across a crater floor. The larger the dune field, the slower its migration, thus DCA may, in some cases, represent a relatively long-term integration of atmospheric activity across a relatively broad area. As with geographic distribution, DCA was extracted from MGD$^3$.

[9] In larger craters, central peaks, younger impacts or erosion may create topographic traps or obstructions within the crater. The resulting crater floor roughness may influence the location of a dune field more than wind direction. DCA is most reliable as an indicator of wind direction when a single dune field occurs within a smooth-floored crater. More than 400 DCAs have been calculated for the 65°N to 65°S region, with ~40 calculated for the 65°N to 90°N region. These include all crater floor types.

#### 3.2.3. Slipface Orientation

[10] The final dune characteristic, SF, is also extracted from MGD$^3$ and used to quantify wind direction. The slipface vector begins on the upwind stoss slope and terminates on the lee slipface slope (Figure 1), indicating the direction of sediment transport and therefore the direction of prevailing winds during the latest period of major dune modification. Detailed study of slipfaces was beyond the scope of a global database, so only gross morphology of dunes formed by unidirectional winds (i.e., barchan, barchanoid and transverse dunes) was used to measure slipface orientation. More than 10,000 raw slipface measurements are included in the 65°N to 65°S region of MGD$^3$, and more than 5,000 in the 65°N to 90°N region. For ease of plotting and comparison to the GCM, individual (raw) slipface azimuths were averaged within each dune field. It is common to have evidence of more than one significant wind direction within a single dune field. When more than one significant direction exists, we calculate an average for each significant wind direction. Slipface orientations are not meant to be used as evidence for current dune activity, nor to imply age constraints, as many of the identified dunes may be inactive.

### 3.3. Mesoscale Study Site

[11] As part of this study, we wanted to select a site where GCM modeled winds, at the closest GCM grid points, were above the 0.0225 N/m$^2$ shear stress threshold. We wanted the winds above the threshold to be in agreement with DCA and in opposition to SF, indicating the possible influence of local, topographically controlled winds. We preferred a

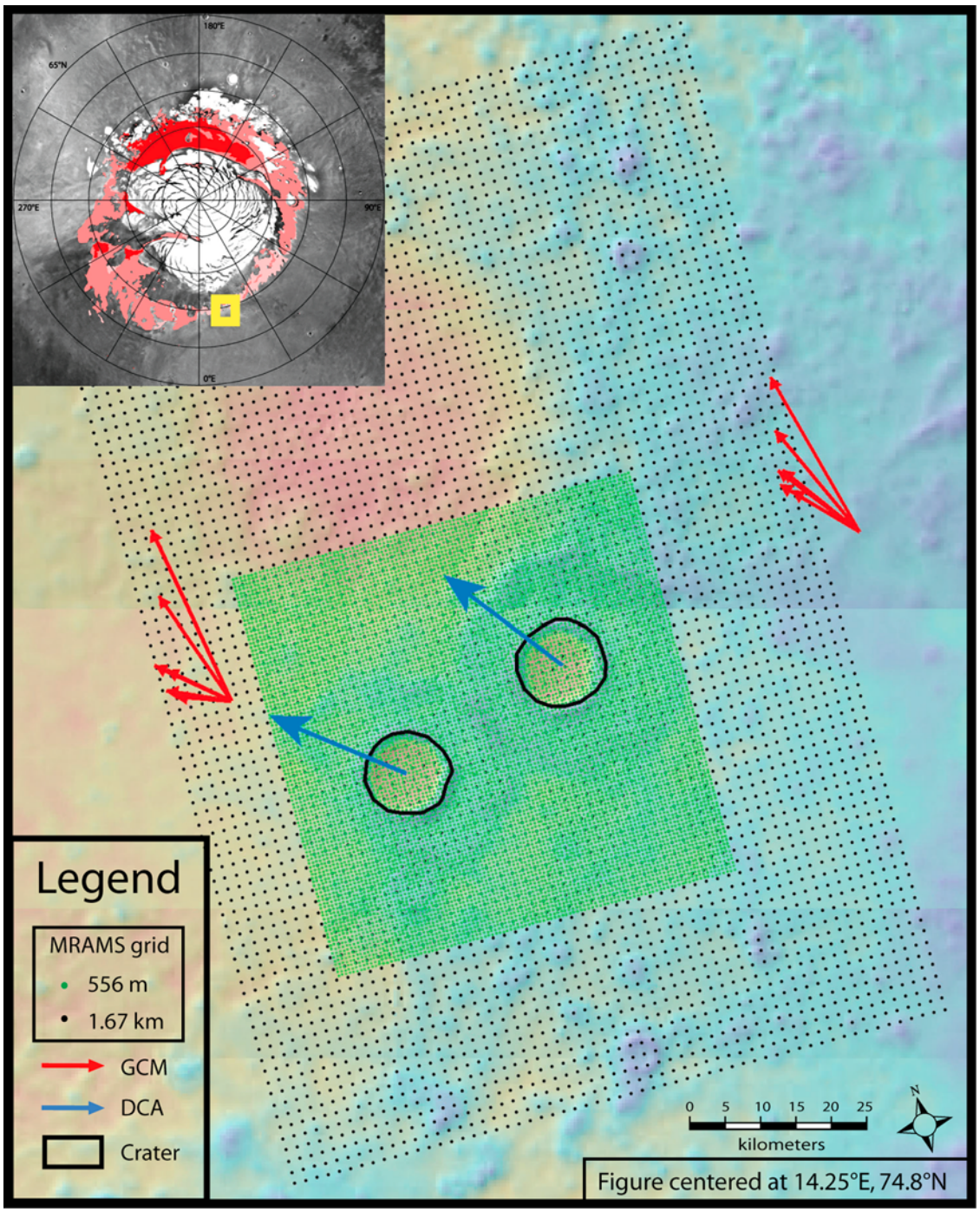


**Figure 2.** Location of mesoscale model study site. North pole inset map shows location of study site (yellow box), residual water ice (white), and dune fields (red and pink). GCM above 10 m/sec at $L_s$ = 167 (red, length of arrows proportional to maximum wind speed), and DCA (blue). Study site shown with MOLA gridded elevation over MOLA hillshade background, elevation ranges from −5000 m (orange) to −4400 m (purple). Polar Stereographic projection.

dune field with multiple SF directions, as further indication of the influence of local winds. We could not find a site that met all of our criteria. The site we chose includes two small craters with DCAs of 280° and 288°, each with an intra-crater dune field displaying multiple SF directions. However, the nearest GCM grid points do not have modeled winds above the shear stress threshold, although several surrounding grid points (within ∼300 km) do produce winds above the shear stress threshold. Six of those grid points with winds above the threshold are north and west of the site and have an average azimuth of 289°. Two are south of the site and have an average azimuth of 39°. At the two grid points nearest the study site (both within ∼60 km), where no winds are above the shear stress threshold, we consider the direction of winds with a velocity >10m/sec (see GCM methods section for more detail). The modeled

winds above the 10 m/sec threshold show a seasonal variation. Approximately 75% blow from east to west, with an average azimuth of 279°, occurring between $L_s$ = 50° and 77° and between $L_s$ = 150° and 190°. The remaining 25% of the modeled winds blow from west to east, with an average azimuth of 104°, and occur between $L_s$ = 92° and 97°. Inspection of the modeled winds showed that the best agreement between GCM and DCA occurred at $L_s$ = 167°. We chose $L_s$ = 167° for the mesoscale model even though TES derived temperatures suggest that $H_2O$ ice may be forming at our study site then, with $CO_2$ ice forming shortly thereafter. The agreement between GCM and DCA suggests an increased possibility that the sand may still be mobile. It is possible that the direction of wind that dominates immediately prior to $CO_2$ ice formation is the direction that is preserved in dune orientation. While we cannot assume that both DCA and SF are controlled by wind at this season, it was a logical place to begin. Figure 2 shows the MRAMS study site area, with the GCM modeled winds above 10m/sec, from $L_s$ = 167° represented by red arrows (length of arrows proportional to maximum wind speed) and DCAs shown by blue arrows. The grid points of the MRAMS model, run to determine whether a mesoscale climate model would better predict SF direction, are represented by small black dots (~1.67 km spacing) and green dots (~556 m spacing).

## 4. Results and Discussion

[12] This section discusses the comparison of the geographic distribution, DCA, and SF of dunes with global output from the Ames Mars GCM and mesoscale output from MRAMS. We begin with the comparison of the geographic distribution to the Ames Mars GCM. For both DCA and SF, we first discuss the comparison to the Ames Mars GCM, then the comparison to MRAMS.

### 4.1. Geographic Distribution

[13] Many factors affect the global pattern of sand deposition and erosion. Attempts have been made to quantify those factors for specific deserts on Earth [e.g., *Kocurek and Havholm*, 1993; *Lancaster*, 1995]. *Kocurek and Lancaster* [1999] describe a sediment state for the Kelso Dunes and the sediment pathway upwind of the dunes. The sediment state is based on sediment supply, sediment availability and the potential of the wind to carry the sand (transport capacity). During the 20,000 years encompassed by their study, wind strength was believed to be fairly consistent and always able to carry the available sand. They concluded that sediment availability controlled aeolian construction. Although sediment supply and sediment availability undoubtedly each play a role on Mars as well, we focus on how the ability of the wind to move sand may affect the geographic distribution of dune fields. A similar approach was taken by *Anderson et al.* [1999], using Viking images. They developed a sand transport model based on the Mars general circulation model (MGCM). Using a threshold stress of 0.024 $N/m^2$, they divided Mars into regions of expected erosion, expected deposition and no change expected. They found that, when compared to Viking-based dune field distribution, their model marginally correlated with dune field location, with 60% of the observed dunes occurring in regions expected to have no change, 25% in areas of expected deposition and 15% in areas of expected erosion. When GCM winds were compared to polar dunes mapped by *Tsoar et al.* [1979], Anderson et al. found a moderate correlation between areas of expected deposition and dunes. We update a global comparison between GCM and dune location, using a more complete inventory of dune fields and a slightly lower GCM threshold. Figure 3 shows that dune fields (shown in shades of red and pink) do not uniformly cover Mars, but are concentrated from 35°S to 80°S and from 70°N to 83°N. Note that dune field outlines have been exaggerated to make small dune fields easier to see, so dune fields appear to cover a larger portion of the surface than is actually covered. Grid points with many winds above the threshold have high sums (larger circles in Figure 3) while grid points with few winds above the threshold have low sums (small circles). Grid points with no winds above the threshold lack circles and roughly correspond to Anderson's areas of no expected change. There seems to be a general pattern, planet-wide, of dunes concentrated where few modeled winds exceed the chosen threshold, while areas with more intense wind activity may have no dunes at all. The area between 55°S and 70°S is an exception. Within that latitudinal band dune fields occur in areas where the shear stress is above the threshold. One place this occurs is on the west side of Argyre Planitia, possibly because terrain here is so rough that sand is easily trapped, even when shear stress values exceed the threshold. Dune fields in the presence of stronger winds also occur just west of Hellas Planitia. Although closer inspection (Figure 4) reveals that most of the dune fields west of Hellas Planitia are deposited in relatively quiet areas adjacent to the higher modeled winds.

[14] Dune deposition in areas that lack winds above the threshold could be due to several factors: 1) the dunes may not have formed under the modeled wind regime (current climate), 2) the GCM's large grid size may have smoothed out small-scale wind gusts, 3) while winds of saltation strength are needed to initiate movement and keep sand moving, too many high winds may keep an area swept clean of sand, with dunes accumulating where winds are less intense, or 4) dune field distribution may be primarily constrained by other factors, such as sediment availability and topographic traps. The anomalous 55°S to 70°S zone may support this last explanation.

### 4.2. Dune Centroid Azimuth

#### 4.2.1. Global Comparison

[15] There are about 340 intracrater dune fields in the equatorial region (65°S to 65°N), whose DCAs were calculated and compared to the GCM. The comparison suggested that agreement varies with diameter of crater, with smaller craters (<25 km diameter) displaying better agreement (~65%) [*Hayward et al.*, 2007a]. We hypothesize that this is because smaller diameter craters tend to have smoother floors and lower rims, allowing unimpeded dune migration, and thus exhibit better correlation between relative dune location and GCM winds. In the north polar region we have only documented about 40 craters containing dune fields. Nearly all are less than 25 km in diameter. For about 70% of these, the DCA agrees fairly well with the GCM modeled wind direction. Figure 5, centered at ~70°N,

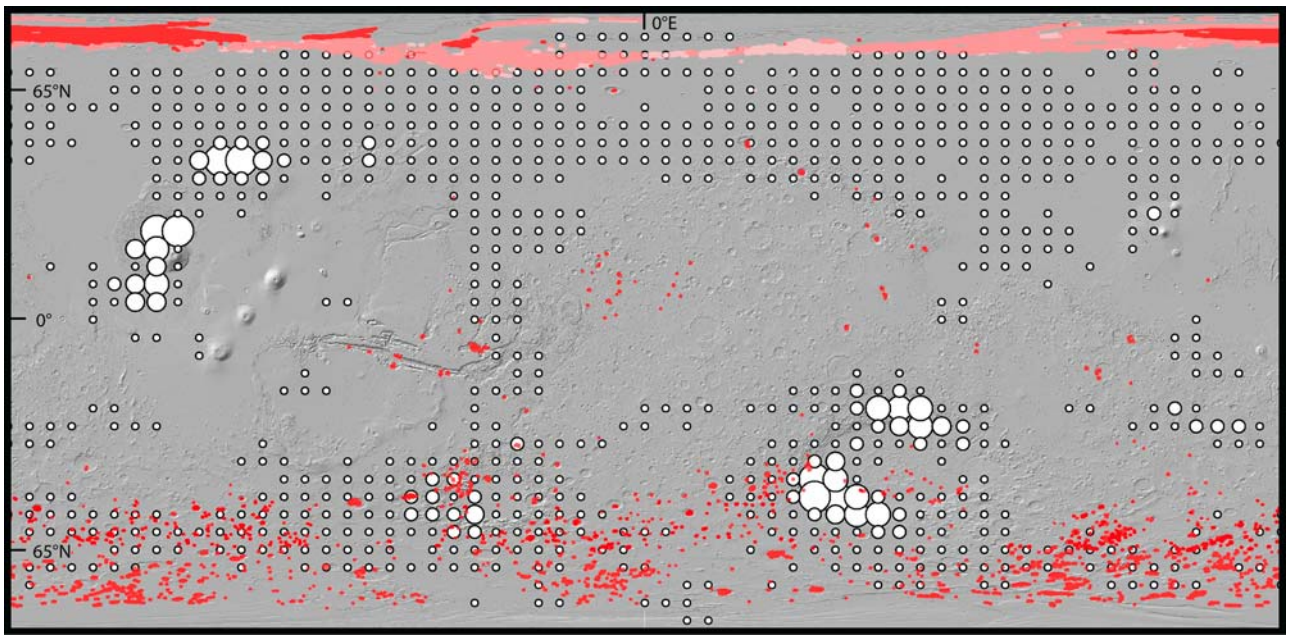


**Figure 3.** Global distribution of dune fields. Dune fields from 65°N to 90°S are shown in red. Dune fields north of 65°N are shown in red where the dunes continuously cover the dune field, reddish-pink where dunes cover less than 80% of the dune field, and pink where dunes are widely scattered within the dune field. Graduated white circles represent the sum of shear stresses (above the 0.0225 N/m$^2$ threshold) at each grid point for one Martian year. Grid points with large circles have higher shear stresses and/or more winds above the threshold. Background is MOLA hillshade. Map is in Equidistant Cylindrical projection and covers 88°S to 88°N.

shows three examples of DCA agreement with GCM modeled winds in the north polar region. Note that winds shown were extracted from an entire Martian year's worth of output, so each grid point potentially has >5,000 modeled winds. Only winds with shear stress > 0.0225 N/m$^2$ when $CO_2$ frost was absent are shown, resulting in only ~5 modeled winds per grid point remaining for comparison. Nearly all of the displayed winds fall within the $L_s$ range of

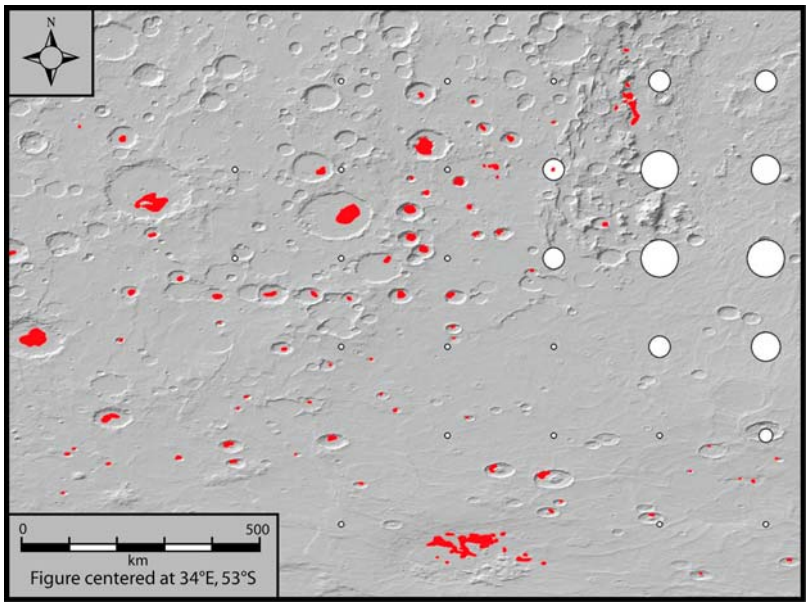


**Figure 4.** Area adjacent to western margin of Hellas Planitia. Detail shows that dune fields (red) are adjacent to higher shear stress area. Graduated white circles represent the sum of shear stresses (above the 0.0225 N/m$^2$ threshold) at each grid point for one Martian year. Grid points with large circles have higher shear stresses and/or more winds above the threshold. Background is MOLA hillshade. Map is in Equidistant Cylindrical projection.

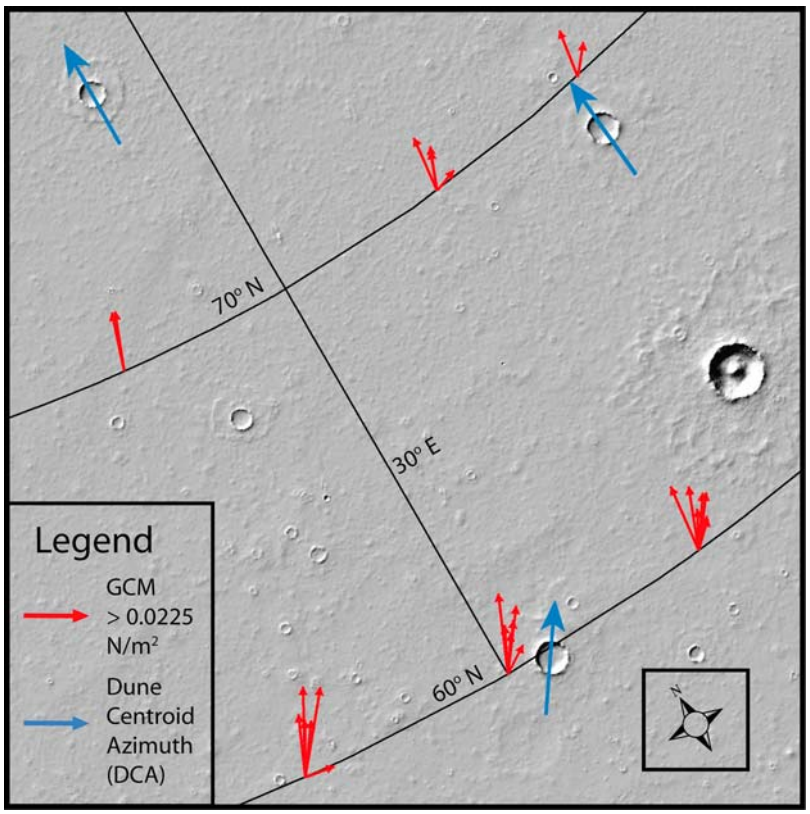


**Figure 5.** Direction of DCA in blue (arrow size increased for visibility), GCM winds over 0.0225 N/m$^2$ for one Martian year in red, with length of arrows proportional to maximum shear stress. MOLA hillshade background. Polar Stereographic projection.

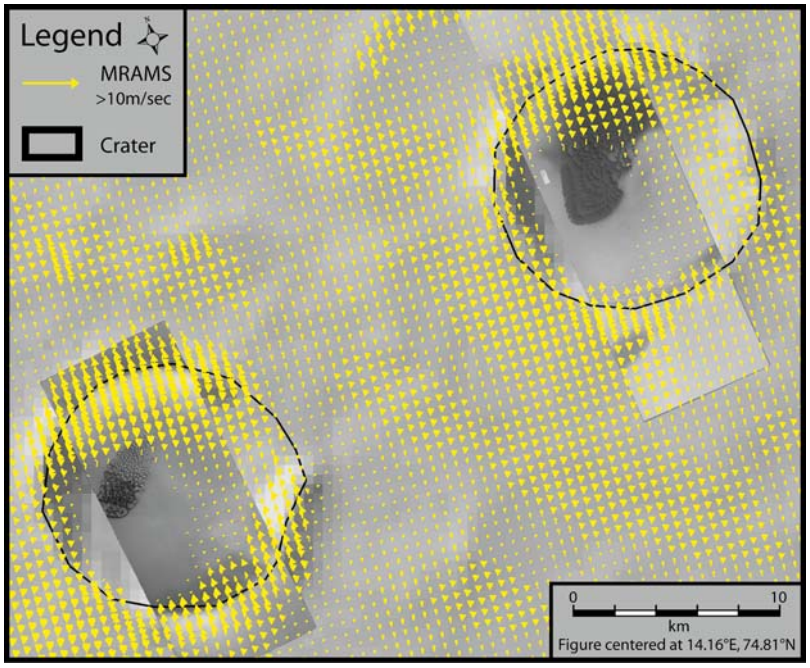


**Figure 6.** MRAMS study site. MRAMS modeled winds (Ls ~ 167°), with magnitude >10 m/sec (yellow), are absent in portions of both craters. Intracrater dune fields occupy parts of these calmer areas. Nearly all modeled winds shown have an azimuth between 225° and 275°. The average wind azimuth for winds >10 m/sec is ~260°. HiRISE images PSP_007584_2550 and PSP_009087_2550. Background is MOLA hillshade. Polar Stereographic projection.

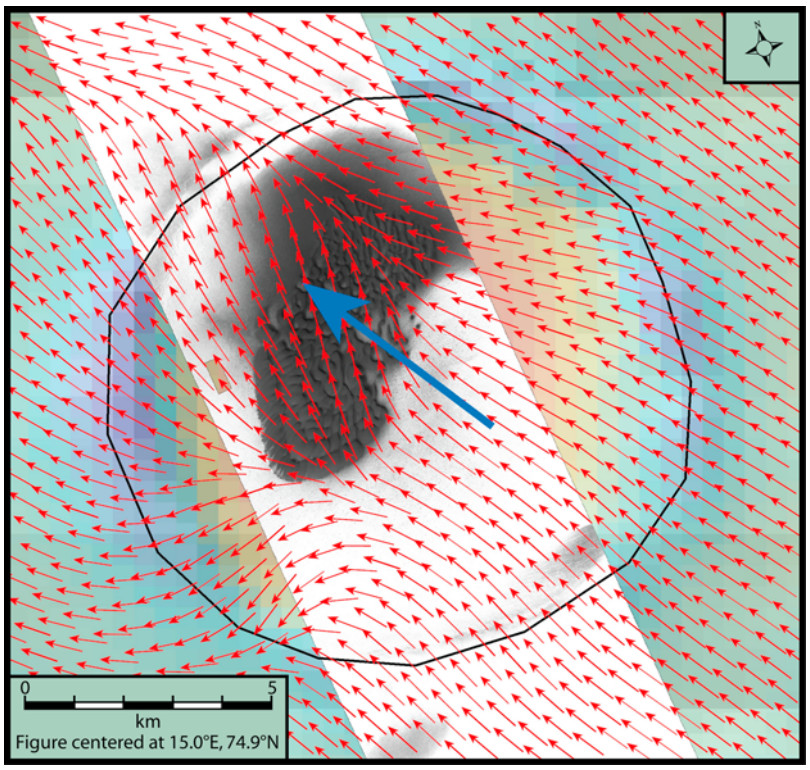


**Figure 7.** Eastern crater at MRAMS study site. MRAMS modeled winds at Ls ~ 167° are represented by red arrows. All magnitudes are shown, including those below the discussed thresholds. Length of arrow does not signify magnitude of wind. LMT = 8.447h. DCA direction (blue) is consistent with modeled winds from the SE. Background is MOLA gridded elevation, overlain by HiRISE image PSP_009087_2550. Polar Stereographic projection.

192° to 211°, and occur between 12.6h and 16.4h local mean time (LMT).

#### 4.2.2. Mesoscale Comparison

[16] As described in the methods section, at our mesoscale study site, we compared GCM modeled winds above 10 m/sec to the DCAs and used the GCM to choose $L_s$ = 167° for our MRAMS modeling. GCM winds from $L_s$ = 167°, shown in Figure 2, agree with the DCA and occurred at no preferred LMT. Figure 6 shows that, for each crater, most of the SW quadrant has no modeled winds greater than 10 m/sec. If the wind patterns from this season were representative of an entire year, the pattern would suggest that saltating sand might be dropped in the calmer SW quadrant. However, seasonal variations doubtless exist [*Fenton et al.*, 2005], which may partially explain why dune fields do not lie entirely within the portions of the craters that are calmer at $L_s$ = 167°. This topographically controlled level of detail is not seen in GCM scale winds. Although the mesoscale modeled winds shown here only span 2 sols, the winds suggest that the relative location of dune fields within craters may be useful as ground truth for mesoscale models. More mesoscale modeling would be needed at different seasons to see if longer term MRAMS modeled wind patterns fully explain dune field location. To determine whether mesoscale wind directions within the calmer regions coincide with DCA, we compare DCA to MRAMS modeled winds of all magnitudes (at $L_s$ = 167°). Figure 7 shows an example, at 8.447 h LMT, when winds align with the general direction of dune migration. While these details are intriguing, conclusions cannot be based on modeled winds from a single $L_s$ and a single LMT. However, we can conclude that the wind regime is far more complicated than the modeled GCM winds suggest, that MRAMS scale is potentially compatible with DCA, and that higher resolution modeling can give us much more realistic detail, especially in topographically complex areas.

### 4.3. Slipface Orientation

#### 4.3.1. Global Comparison

[17] When comparing SF to GCM winds in the equatorial region, we found that agreement (~40%) was not as good as that of DCA and GCM winds (~65%), possibly because the crater walls affect local winds, and therefore dune morphology. A logical test of this would be to look at intercrater dunes. They are scarce in the equatorial region, but do show a somewhat better correlation (50%) to the GCM output. In the north polar region, for intracrater dunes, the SF to GCM agreement rate is only about 40%. For dunes in the circumpolar erg, agreement is very good in some areas, especially in the southern part of the erg (70°N to 75°N) between 250°E and 340°E. A notable exception occurs when slipface evidence suggests that winds locally funnel down chasmata. The GCM does not reflect this because the model grid spacing is too coarse to spatially resolve features, such as the chasmata, on Planum Boreum.

#### 4.3.2. Mesoscale Comparison

[18] MRAMS modeled winds show that the topography of the craters greatly affects diurnal changes in wind flow

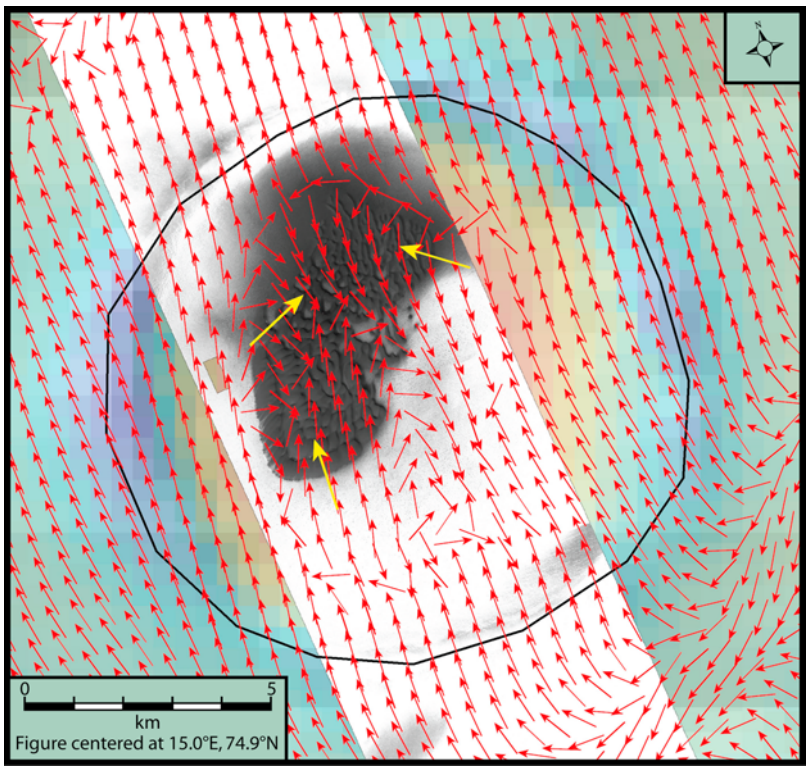


**Figure 8.** Eastern crater at MRAMS study site. MRAMS modeled winds at Ls ~ 167° are represented by red arrows. All magnitudes are shown, including those below the discussed thresholds. Length of arrow does not signify magnitude of wind. LMT = 0.781h. Average SF directions (yellow) are consistent with modeled winds from the SSE, SW, and ESE. Background is MOLA gridded elevation, overlain by HiRISE image PSP_009087_2550. Polar Stereographic projection.

direction. Modeled winds in the late afternoon to evening hours agree, for short periods of time, with SF direction. Figure 8 shows the dune field in the eastern crater of the study site. Three SF directions, averaged from ~100 measured SFs, are shown in yellow. At this time of night, 0.781h LMT, the wind pattern is complex, showing some agreement with all three SF directions. However, as discussed in the preceding paragraph, the winds near the dune field are extremely weak and could probably not transport sand. The fact that modeled wind directions, though weak, sometimes agree with the varied SF directions is encouraging. We theorize that a change in season or climate may result in stronger winds, although confirming this would require many more computationally expensive MRAMS simulations than is feasible for the present work. However, even if significantly stronger winds were not predicted by the mesoscale model, it is important to understand that the winds modeled using a grid spacing of ~556 m are still spatial mean values (implicitly spatially averaged over $\sim 556^2$ $m^2$), and such a grid spacing is not able to resolve the turbulent boundary layer structure/processes that may result in sporadic turbulent gusts (along with vortices such as dust devils) of significant magnitude. Such unsteady turbulent magnification of the wind can occur both at night (particularly near topographic obstacles) and during the day (nearly anywhere that is sunlit). Evidence that such small-scale, stochastic gusts occur includes the sporadic events that have cleaned significant amounts of accumulated dust from the decks of the MER rovers [*Sullivan et al.*, 2008], and the sand movement observed by HiRISE images and the MER rover Opportunity near Victoria crater [e.g., *Bridges et al.*, 2007]. In both of these examples, mesoscale model runs [e.g., *Rafkin and Michaels*, 2003] have indicated no propensity for particle saltation. *Fenton and Michaels* [2008] demonstrated that when MRAMS indicated no particle entrainment should occur, convective activity modeled in MRAMS large eddy simulation (LES) produced winds above an estimated saltation threshold. On Earth, *McKenna Neuman et al.* [2000] made rapid (10s) measurements of sediment transport and wind speed on the stoss side of a dune. They found that wind gusts of short duration, associated with turbulence, moved very little sediment and contributed very little to dune modification. However, on Mars, where the atmospheric density is much lower, sand may only move through infrequent events in which the mean wind is enhanced by turbulence. The few wind events that cleaned Spirit and Opportunity's solar panels and caused ripple movement may be examples of turbulence enhanced mean winds. We have observed (in Mars microscale modeling work) that the strongest dry convective gusts (associated with the leading edge of convective cells; dust devils excluded) travel in the same direction as the mean wind. In the absence of mean winds that can saltate particles and in the absence of any other significant process that can destroy piles of sand faster than they can be built up, gusts may be able to produce organized dune patterns. Atmospheric models are just beginning to resolve turbulence.

Modeling turbulent flow in our study area may help explain the presence and orientation of the intracrater dunes.

## 5. Summary

[19] Three possible records of atmosphere/surface interaction are presented here; geographic distribution of dune fields, DCA, and SF. The geographic distribution of dune fields may be a broad brush indicator of long-term regional atmospheric trends, making it valuable as ground truth for GCMs. Concentrations of dune fields are highest north of 70°N and south of about 35°S, which indicates that in these areas 1) a sand source was available, 2) atmospheric activity was great enough to allow sand transport, and 3) where dune fields are now located, atmospheric activity dropped enough to cause the sand load to be deposited. Dune Centroid Azimuth (DCA), when calculated for dunes in smooth-floored craters, agrees moderately well with GCM wind directions. DCA may be a fairly reliable record of regional (GCM scale) atmospheric activity for the southern hemisphere, where intracrater dunes dominate. Mesoscale modeled winds retain much of the regional (GCM) signal, while incorporating the effects of crater topography. Thus DCA can be valuable as ground truth for both GCM and mesoscale models. Agreement between Slipface Orientation (SF) and GCM wind directions in intracrater dune fields is not as strong as between DCA and GCM wind directions, suggesting that crater topography may influence local winds that control slipface development. Where local topography is less important (e.g., parts of the north polar erg) SF may more closely reflect the regional wind regime. Modeled winds at our MRAMS study area showed topographically controlled diurnal fluctuations on a scale (grid spacing ~550 m) that would be appropriate for comparison to SF. Furthermore, at 0.781h LMT, MRAMS wind directions were partially consistent with observed SF directions. Limitations inherent in having only two sols of MRAMS output, combined with a lack of MRAMS winds above saltation strength, lead to inconclusive results. However, even with these limitations, our study demonstrates that MRAMS is capable of modeling wind variability that may be consistent with observed complex SF patterns. Thus we are encouraged that SF may be useful in testing such mesoscale models. More MRAMS modeling is needed, at different seasons and obliquities, or with LES to evaluate the usefulness of SF as mesoscale ground truth.

## 6. Future Work

[20] Although agreement between our observations and modeled wind directions are encouraging, the lack of strong modeled winds in dune fields needs further investigation. MRAMS modeling at different seasons or at different orbit/axis conditions may reveal higher winds, more capable of forming dunes, and modeling that includes LES may demonstrate that turbulence plays an important role in moving sand. With more complete modeling, we could better assess the value of dunes as ground truth. In addition, expansion of the database to include a broader scope of aeolian features that form on different time scales (e.g., transverse aeolian ridges, yardangs, ventifacts, wind streaks and dust devil tracks) would make the database a more powerful tool for atmospheric modelers.

[21] **Acknowledgments.** We appreciate the thoughtful reviews by Ken Herkenhoff and Paul Geissler and Circe Verba's assistance with HiRISE images. We would also like to thank an anonymous reviewer for suggestions that assisted in improving the manuscript. This project was partially supported as part of the Mars Odyssey Thermal Emission Imaging Spectrometer Project (Arizona State University). Any use of trade or product names in this publication is for descriptive purposes only and does not imply endorsement by the U.S. government.

## References

Anderson, F. S., R. Greeley, P. Xu, E. Lo, D. G. Blumberg, R. M. Haberle, and J. R. Murphy (1999), Assessing the Martian surface distribution of aeolian sand using a Mars general circulation model, *J. Geophys. Res.*, *104*(E8), 18,991–19,002, doi:10.1029/1999JE900024.

Bourke, M. C., J. Bullard, and O. Barnouin-Jha (2004), Aeolian sediment transport pathways and aerodynamics at troughs on Mars, *J. Geophys. Res.*, *109*, E07005, doi:10.1029/2003JE002155.

Bridges, N. T., P. E. Geissler, A. S. McEwen, B. J. Thomson, F. C. Chuang, K. E. Herkenhoff, L. P. Keszthelyi, and S. Matinez-Alonso (2007), Windy Mars: A dynamic planet as seen by the HiRISE camera, *Geophys. Res. Lett.*, *34*, L23205, doi:10.1029/2007GL031445.

Christensen, P. R., et al. (2004), The Thermal Emission Imaging System (THEMIS) for the Mars 2001 Odyssey Mission, *Space Sci. Rev.*, *110*, 85–130, doi:10.1023/B:SPAC.0000021008.16305.94.

Cutts, J. A., and R. S. U. Smith (1973), Aeolian deposits and dunes on Mars, *J. Geophys. Res.*, *78*, 4139–4154, doi:10.1029/JB078i020p04139.

Edgett, K. S., and M. C. Malin (2000), MGS MOC images of Seif dunes in the north polar region of Mars, *Lunar Planet. Sci.*, *XXXI*, Abstract 1070.

Fenton, L. K., and T. I. Michaels (2008), Characterizing daytime erosion potential on Mars using the MRAMS LES, *Lunar Planet. Sci.*, *XXXIX*, Abstract 1964.

Fenton, L. K., M. I. Richardson, and A. D. Toigo (2002), Sand transport in Proctor Crater on Mars based on dune morphology and mesoscale modeling, *Lunar Planet. Sci.*, *XXXIII*, Abstract 1953.

Fenton, L. K., J. L. Bandfield, A. W. Ward, and A. Wesley (2003), Aeolian processes in Proctor Crater on Mars: Sedimentary history as analyzed from multiple data sets, *J. Geophys. Res.*, *108*(E12), 5129, doi:10.1029/2002JE002015.

Fenton, L. K., A. D. Toigo, and M. I. Richardson (2005), Aeolian processes in Proctor Crater on Mars: Mesoscale modeling of dune-forming winds, *J. Geophys. Res.*, *110*, E06005, doi:10.1029/2004JE002309.

Fryberger, S. G., and T. S. Ahlbrandt (1979), Mechanisms for the formation of aeolian sand seas, *Z. Geomorphol.*, *23*, 440–460.

Greeley, R., A. Skypeck, and J. B. Pollack (1993), Martian aeolian features and deposits: Comparison with general circulation model results, *J. Geophys. Res.*, *98*(E2), 3183–3196, doi:10.1029/92JE02580.

Greeley, R., et al. (2006), Gusev crater: Wind-related features and processes observed by the Mars Exploration Rover Spirit, *J. Geophys. Res.*, *111*, E02S09, doi:10.1029/2005JE002491.

Greeley, R., et al. (2008), Columbia Hills, Mars: Aeolian features seen from the ground and orbit, *J. Geophys. Res.*, *113*, E06S06, doi:10.1029/2007JE002971.

Haberle, R. M., M. M. Joshi, J. R. Murphy, J. R. Barnes, J. T. Schofield, G. Wilson, M. Lopez-Valverde, J. L. Hollingsworth, A. F. C. Bridger, and J. Schaeffer (1999), General circulation model simulations of the Mars Pathfinder atmospheric structure investigation/meterology data, *J. Geophys. Res.*, *104*(E4), 8957–8974, doi:10.1029/1998JE900040.

Haberle, R. M., J. R. Murphy, and J. Schaeffer (2003), Orbital change experiments with a Mars general circulation model, *Icarus*, *161*, 66–89, doi:10.1016/S0019-1035(02)00017-9.

Hayward, R. K., K. F. Mullins, L. K. Fenton, T. M. Hare, T. N. Titus, M. C. Bourke, A. Colaprete, and P. R. Christensen (2007a), Mars Global Digital Dune Database and initial science results, *J. Geophys. Res.*, *112*, E11007, doi:10.1029/2007JE002943.

Hayward, R. K., K. F. Mullins, L. K. Fenton, T. M. Hare, T. N. Titus, M. C. Bourke, T. Colaprete, and P. R. Christensen (2007b), Digital database of dunes on Mars, *U. S. Geol. Surv. Open File Rep., 2007–1158*.

Hayward, R. K., L. K. Fenton, K. L. Tanaka, T. N. Titus, A. Colaprete, and P. R. Christensen (2008), Aeolian features as ground truth for atmospheric modeling on Mars, in *Third International Workshop on The Mars Atmosphere: Modeling and Observations*, *LPI Contrib. 1447*, p. 9033.

Kocurek, G., and K. G. Havholm (1993), Eolian sequence stratigraphy-a conceptual framework, in *Siliciclastic Sequence Stratigraphy*, edited by

P. Weimer and H. Posamentier, pp. 393–409, Am. Assoc. of Pet. Geol., Tulsa, Okla.

Kocurek, G., and N. Lancaster (1999), Aeolian sediment states: Theory and Mojave Desert Kelso Dunefield example, *Sedimentology*, *46*(3), 505–516, doi:10.1046/j.1365-3091.1999.00227.x.

Lancaster, N. (1995), *Geomorphology of Desert Dunes*, 290 pp.Routledge, London.

Malin, M. C., G. E. Danielson, A. P. Ingersoll, H. Masursky, J. Veverka, M. A. Ravine, and T. A. Soilanille (1992), Mars observer camera, *J. Geophys. Res.*, *97*(E5), 7699–7718, doi:10.1029/92JE00340.

Malin, M. C., et al. (1998), Early views of the Martian surface from the Mars orbiter camera of Mars Global Surveyor, *Science*, *279*, 1681–1685, doi:10.1126/science.279.5357.1681.

McCauley, J. F., M. H. Carr, J. A. Cutts, W. K. Hartmann, H. Masursky, D. J. Milton, R. P. Sharp, and D. E. Wilhelms (1972), Preliminary Mariner 9 report on the geology of Mars, *Icarus*, *17*, 289–327, doi:10.1016/0019-1035(72)90003-6.

McEwen, A. S., et al. (2007), Mars Reconnaissance Orbiter's High Resolution Imaging Science Experiment (HiRISE), *J. Geophys. Res.*, *112*, E05S02, doi:10.1029/2005JE002605.

McKenna Neuman, C., N. Lancaster, and G. Nickling (2000), The effect of unsteady winds on sediment transport on the stoss slope of a transverse dune, Silver Peak, Nevada, *Sedimentology*, *47*(1), 211–226, doi:10.1046/j.1365-3091.2000.00289.x.

Michaels, T. I. (2008), Unlocking the environmental conditions recorded by aeolian bedforms with the aid of high-resolution atmospheric modeling, *Planetary Dunes Workshop: A Record of Climate Change, LPI Contrib. 1403*, 52–53.

Rafkin, S. C. R., and T. I. Michaels (2003), Meteorological predictions for 2003 Mars Exploration Rover high-priority landing sites, *J. Geophys. Res.*, *108*(E12), 8091, doi:10.1029/2002JE002027.

Rafkin, S. C. R., R. M. Haberle, and T. I. Michaels (2001), The Mars regional atmospheric modeling system: Model description and selected simulations, *Icarus*, *151*, 228–256, doi:10.1006/icar.2001.6605.

Sullivan, R., et al. (2008), Wind-driven particle mobility on Mars: Insights from Mars Exploration Rover observations at "El Dorado" and surroundings at Gusev Crater, *J. Geophys. Res.*, *113*, E06S07, doi:10.1029/2008JE003101.

Thomas, P. (1982), Present wind activity on Mars: Relation to large latitudinally zoned sediment deposits, *J. Geophys. Res.*, *87*, 9999–10,008, doi:10.1029/JB087B12p09999.

Tsoar, H., R. Greeley, and A. R. Peterfreund (1979), Mars: The north polar sand sea and related wind patterns, *J. Geophys. Res.*, *84*, 8167–8180, doi:10.1029/JB084iB14p08167.

Ward, A. W. (1979), Yardangs on Mars: Evidence of recent wind erosion, *J. Geophys. Res.*, *84*, 8147–8166, doi:10.1029/JB084iB14p08147.

Ward, A. W., K. B. Doyle, P. J. Helm, M. K. Weisman, and N. E. Witbeck (1985), Global map of eolian features on Mars, *J. Geophys. Res.*, *90*(B2), 2038–2056, doi:10.1029/JB090iB02p02038.

Wilson, S. A., and J. R. Zimbelman (2004), Latitude-dependent nature and physical characteristics of transverse aeolian ridges on Mars, *J. Geophys. Res.*, *109*, E10003, doi:10.1029/2004JE002247.

P. R. Christensen, Department of Geological Sciences, Arizona State University, Tempe, AZ 85287, USA.

A. Colaprete, NASA Ames Research Center, Moffett Field, CA 94035, USA.

L. K. Fenton, Carl Sagan Center, Moffett Field, CA 94043, USA.

R. K. Hayward and T. N. Titus, U.S. Geological Survey, 2255 North Gemini Dr., Flagstaff, AZ 86001, USA.

T. I. Michaels, Southwest Research Institute, 1050 Walnut St., Boulder, CO 80302, USA.